

Experimental Chiral Dynamics: New Opportunities with Polarized Internal Targets and Almost-Real Photon Tagging

A.M. Bernstein and M.M. Pavan
 Physics Department and Laboratory for Nuclear Science
 M.I.T., Cambridge, MA, U.S.A.

Abstract

Experiments on pion (Goldstone Boson) photoproduction from the nucleon tests the ability to make QCD predictions at confinement scale energies. Experiments with both polarized beams and targets have the potential sensitivity to demonstrate the dynamic isospin breaking effects of the up and down quark mass differences, whereas experiments on Compton scattering from the nucleon will incisively probe its chiral structure by measuring all of the spin dependent amplitudes. These and other types of photo-induced measurements on nuclei could be possible at BLAST with the addition of an almost-real photon tagging system and a forward low energy recoil ion hodoscope.

1 Confinement Scale QCD and Chiral Dynamics

At low energies the interaction between quarks and gluons is extremely strong and leads to confinement, where approximate QCD solutions can be obtained by an effective field theory known as chiral perturbation theory (ChPT) or Chiral Dynamics[1, 2, 3, 4]. This is based on the chiral symmetry present in the QCD Lagrangian in the limit of massless light quarks, but which is broken in the ground state of matter. In such a situation, Goldstone's theorem states that there are massless, pseudoscalar Bosons whose interactions with other hadrons vanish at zero momentum[1, 5, 6]. In the case of $m_u=m_d=0$, there are three Goldstone Bosons which are identified as the pion triplet. The relatively weak interactions of Goldstone Bosons at low energies invites a perturbation scheme based on chiral symmetry and hadronic degrees of freedom.

In the real world, the light quark masses are nonzero, but small [7, 8]. Therefore, for strong interaction theory to have predictive power, calculations must be performed taking the deviations from the pure Goldstone theorem into account. As an example, the s wave scattering length, a , vanishes for a Goldstone Boson scattering from any hadron in the low energy limit. However for a physical meson with finite mass (π, η, K) one would intuitively expect $a \simeq 1/\Lambda_x$ (see contribution of A.B. in Ref.[4]) where Λ_x is the chiral symmetry breaking scale ($\simeq 4\pi f_\pi \simeq 1\text{GeV}$ for pions, where $f_\pi = 92.4\text{MeV}$ is the decay constant). This intuitive expectation is supported by the original calculation of Weinberg [9] in which the scattering lengths of pions from any hadrons were first obtained by current algebra techniques (a precursor of ChPT). The order of magnitude of the s wave scattering lengths is[9]:

$$a_o = \frac{m_\pi}{4\pi f_\pi^2} = \frac{m_\pi}{\Lambda_x f_\pi} \simeq \frac{1.5}{\Lambda_x} \quad (1)$$

One observes that $a_o \rightarrow 0$ when $m_\pi \rightarrow 0$ (the chiral limit) and also that $a_o \simeq 1/\Lambda_x$.

Similarly, one would expect the production and decay amplitudes of Goldstone Bosons to vanish in the chiral limit. Some examples, which can be obtained from ChPT calculations [2, 3], are the threshold electric dipole amplitude, $E_{0+}^{\gamma N \rightarrow \pi^0 N}$ for s wave photo-pion production, the Σ term of πN scattering, the isospin breaking $\eta \rightarrow 3\pi$ decay, and the form factors for K_{l4} decays. In a similar vein, there are some observables that diverge in the chiral limit, such as the charge radii and polarizabilities of nucleons and pions [2, 3]. In this case, the physical interpretation is that the meson cloud extends beyond the hadron and in the chiral limit extends to infinity.

Pion-hadron scattering and the amplitudes given above are examples of quantities that either vanish or blow up in the chiral limit. In the real world, where the light quark masses are non-zero, chiral symmetry is explicitly broken and these quantities are finite and non-zero. Their precise (nonzero and finite) values are measures of explicit chiral symmetry breaking, and therefore a theoretical challenge to calculate them. Quantities which either vanish or diverge in the chiral limit point to an experimental opportunity to perform precise experiments, not only to check ChPT calculations, but also as fundamental quantities which must be predicted by any theory of the strong interaction. Experimental Chiral Dynamics is the study of the properties, production and decay amplitudes, and low energy interactions of the almost Goldstone Bosons (π, η, K) with themselves and with other hadrons.

The main purpose of this contribution is to point out new and exciting experimental possibilities in chiral dynamics which arise by having an experimental apparatus with thin, pure, polarized, targets in an electron storage ring with an intense, polarized, electron beam of $\simeq 1$ GeV. We will introduce the possibility of a new very small angle electron scattering/almost-real photon tagging facility (SMASH) which will utilize the polarized, internal targets being built for BLAST. As important examples we shall discuss the threshold $\vec{\gamma}p \rightarrow \pi^0 p$ and polarized Compton scattering, $\vec{\gamma}\vec{p} \rightarrow \gamma p$, reactions. Furthermore, such a facility would be capable of measuring all photo-hadron processes with polarized photons on polarized and unpolarized internal targets, e.g. protons, deuterons, and 3He . In particular, the coherent $\vec{\gamma}\vec{D} \rightarrow \pi^0 D$ reaction can be accessed from threshold through the Δ region and could produce important new results on the $\vec{\gamma}\vec{n} \rightarrow \pi^0 n$ amplitude. Some of these experiments require soft recoil ion detection near the internal target. We will also point out the possibility of using the BLAST detector itself in addition to the internal target to investigate other timely physics issues e.g. to study the quadrupole components in the $\vec{\gamma}\vec{p} \rightarrow \Delta$ transition.

1.1 Photopion Reactions and Light Quark Dynamics

Near threshold pion photoproduction is an excellent example of confinement scale QCD physics, where considerable theoretical and experimental progress has been made in the past few years. Starting with the availability of CW electron beams, the $\gamma p \rightarrow \pi^0 p$ reaction has

been performed with high quality tagged photon beams at Mainz[10] and Saskatoon[11]. At the same time, ChPT calculations have been performed which have advanced our understanding of this reaction[12]. For the sake of brevity only the photoproduction experiments will be discussed here.

ChPT is an effective field theory which uses the observed hadrons rather than the quarks and gluons as the degrees of freedom[1, 2, 3, 4]. The effective Lagrangians are organized into a series of increasing powers of the momenta, $(p/\Lambda_x)^n$, where $\Lambda_x \simeq 4\pi f_\pi \simeq 1\text{GeV}$ is the chiral scale parameter. The introduction of a higher order Lagrangian introduces low energy constants which are required to renormalize the infinities order by order. At the present time these low energy constants must be determined empirically by fits to data or estimated by the principle of resonance saturation. In principle they can be obtained from the QCD Lagrangian by integrating out the high energy degrees of freedom, e.g. by lattice gauge theory. The importance of ChPT is that it is an effective *theory* based on QCD, i.e. at each order in the momentum expansion, the diagrams that must be calculated are specified and not left to individual discretion as they are in model calculations.

At the present time one loop ChPT calculations for electromagnetic pion production have been carried out to $O(p^4)$ [12]. The presence of the counterterms implies 3 low energy constants in photoproduction and 5 in electroproduction: two in the transverse s wave multipole E_{0+} , one in the p wave transverse multipoles, and two in the longitudinal s wave multipole L_{0+} (for electroproduction). Currently, these are determined by a fit to the data and also estimated by the principle of resonance saturation. The two approaches are found to agree [12], indicating that the values are understood. It should also be noted that π^0 photo and electroproduction from the neutron can be predicted without any additional parameters. Thus measurements of the neutron production amplitudes will provide a stringent test of ChPT calculations.

One important advantage that ChPT has brought to the study of electromagnetic meson production is the systematic ordering of the diagrams. In particular, pion rescattering in the final state (1 loop diagram) is the crucial ingredient of the near threshold energy dependence. The largest contribution comes from the production of charged pions in the intermediate state. Since the ratio of the electric dipole amplitudes for the neutral and charged pion channels $R = E_{0+}^{\gamma p \rightarrow \pi^+ n} / E_{0+}^{\gamma p \rightarrow \pi^0 p} \simeq -20$, the two step $\gamma p \rightarrow \pi^+ n \rightarrow \pi^0 p$ reaction is as strong as the direct $\gamma p \rightarrow \pi^0 p$ path. Combined with the separation of the $\pi^0 p$ and $\pi^+ n$ thresholds this leads to a unitary cusp in the $\gamma p \rightarrow \pi^0 p$ reaction.

The simplest example to understand the occurrence of the unitary cusp in the $\gamma^* p \rightarrow \pi^0 p$ reaction (where γ^* is a real or virtual photon) is to use the 3 channel S matrix for the open channels $(\gamma^* p, \pi^0 p, \pi^+ n)$ [13]. Applying the constraints of unitary and time reversal invariance, one is led to the coupled channel result for the s wave amplitude $E_{0+}^{\gamma p \rightarrow \pi^0 p}$:

$$E_{0+}^{\gamma p \rightarrow \pi^0 p}(k) = e^{i\delta_0} [A(k) + i\beta q_+] \quad (2)$$

where δ_0 is the s wave $\pi^0 p$ phase shift (predicted to be very small), $A(k)$ is a smooth function

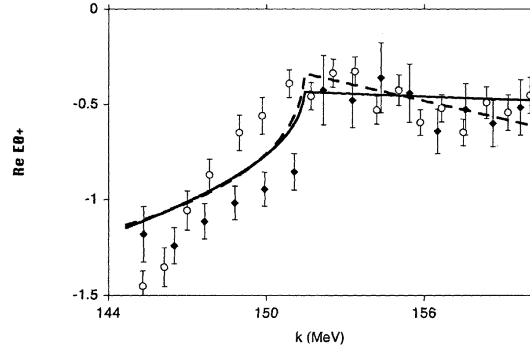


Figure 1: $Re E_{0+}$ (in units of $10^{-3}/m_\pi$) for the $\gamma p \rightarrow \pi^0 p$ reaction versus photon energy k . The dashed dot curve is the ChPT fit [2] and the solid curve is the unitary fit Eq. 2 to the Mainz [10] data (open circles). The Saskatoon data [11] is also shown (filled circles).

of the photon energy k , $\beta = E_{0+}^{\gamma p \rightarrow \pi^+ n} \cdot a_{\pi^+ n \rightarrow \pi^0 p}^{ceex}$ is the cusp parameter, and q_+ is the π^+ CMS momentum which is continued below the $\pi^+ n$ threshold as $i |q_+|$. The cusp function βq_+ contributes to the real (imaginary) part of E_{0+} below (above) the $\pi^+ n$ threshold.

The results for the real part of the s wave electric dipole amplitude $E_{0+}^{\gamma p \rightarrow \pi^0 p}$ are presented in Fig. 1. The rapid energy dependence between the $\pi^0 p$ and $\pi^+ n$ thresholds at 144.7 and 151.4 MeV due to the unitary cusp can be seen. Above the $\pi^+ n$ threshold the energy dependence is much less rapid. This is in approximate agreement with the predictions of the unitary cusp (Eq.2, Ref.[13]) and ChPT[12]. It should be noted that the errors in the data shown in Fig.1 are statistical only so that the disagreement between the data sets is not serious. To complete the observation of the unitary cusp and to precisely measure the value of β , $Im(E_{0+})$ must be measured. In particular, experiments with polarized targets can measure the predicted rapid rise in $Im(E_{0+}^{\gamma p \rightarrow \pi^0 p})$ above the $\pi^+ n$ threshold. The SMASH facility outlined here would provide such important data.

The unitary constraints to the multipole amplitudes show the importance of the final state πN scattering and charge exchange on the $\gamma^* p \rightarrow \pi^0 p$ reaction. It raises the possibility of measuring $a_{\pi^0 p}$ and $a_{\pi^+ n \rightarrow \pi^0 p}^{ceex}$ by measurements of $Im(E_{0+}^{\gamma p \rightarrow \pi^0 p})$ both below and above the $\pi^+ n$ threshold[13]. The s wave $\pi^0 N$ elastic scattering and charge exchange scattering length have been of considerable interest since Weinberg[7] predicted that there should be an isospin breaking effect due to the up, down quark mass difference. For $a_{\pi^0 N}$ this effect is $\simeq 30\%$, in large part because the isospin conserving term in $a_{\pi^0 N}$ is very small ($\simeq 0.01/m_\pi$) and consequently very difficult to measure. Since the charge exchange scattering length is much larger ($\simeq 0.13/m_\pi$) this is easier to observe. Here the isospin violating term due to the up and down quark mass effect is the same (within a factor of $\sqrt{2}$) of the elastic scattering prediction but in relative terms is $\simeq 2$ to 3% of the isospin conserving term. The most straightforward way to observe this predicted isospin violation is to measure the cusp parameter β in the $\gamma p \rightarrow \pi^0 p$ reaction with polarized proton targets[13] and also E_{0+} in

the $\gamma p \rightarrow \pi^+ n$ reaction. Then one could compare the values of $a_{\pi^+ n \rightarrow \pi^0 p}^{ceex}$ with the measured value of $a_{\pi^- p \rightarrow \pi^0 n}^{ceex}$ from the line width in pionic hydrogen[14]. If isospin is a good quantum number then these will be equal and opposite. Equivalently, the dynamic isospin breaking effect of the up, down quark masses can be considered as an isospin breaking contribution to β of $\simeq 2$ to 3% [13].

In addition to the s wave multipole E_{0+} discussed above, ChPT makes predictions for the threshold magnitudes of the three p wave multipoles (P_1, P_2, P_3)[12]. Since the p wave πN phase shifts are small at low energies, the p wave multipoles are essentially real. Therefore for each threshold $\gamma N \rightarrow \pi N$ reaction there are five multipole amplitudes to be measured ($Re(E_{0+}), Im(E_{0+}), P_1, P_2, P_3$). The unpolarized cross section can be written as $\sigma(\theta) = A + B\cos(\theta) + C\cos^2(\theta)$ where A, B, and C are real bilinear combinations of the five multipole amplitudes[12, 15]. A complete experimental determination of the multipoles requires then two additional polarization measurements. This could include, e.g. measurements with linear polarized photons and unpolarized targets and with polarized targets and unpolarized photons (this latter response measures imaginary parts of interference amplitudes[15]). Measurements with both photon and target polarization could also be used[15]. There are three independent isospin amplitudes and four reaction channels ($\gamma p \rightarrow \pi^+ n, \gamma p \rightarrow \pi^0 p, \gamma n \rightarrow \pi^- p, \gamma n \rightarrow \pi^0 n$). so a measurement of all four constitutes a test of isospin conservation. Therefore, a comprehensive set of measurements of the threshold photo-pion reactions requires experiments with polarized photons and targets, including both neutron and proton targets. Unpolarized experiments on the threshold $\gamma p \rightarrow \pi^0 p$ reaction have been performed [10, 11]. The results for the s wave multipole E_{0+} were discussed above. In addition, two linear combinations of the three p wave multipoles were found to be in agreement with ChPT calculations [12, 10, 11]. More recently we have performed a threshold $\vec{\gamma} p \rightarrow \pi^0 p$ experiment at Mainz with linearly polarized photons and the data are presently being analyzed. This will complete the measurement of the three p wave multipoles for π^0 photoproduction from the proton. However at the present time, there are no measurements of $Im(E_{0+})$, which requires polarized target experiments such as can be performed at SMASH.

There is also growing interest in using the deuteron as a neutron target for the $\gamma n \rightarrow \pi N$ amplitudes. A ChPT calculation for the coherent $\gamma D \rightarrow \pi^0 D$ reaction exactly at threshold has been performed[16], as was a first experiment of the $\gamma D \rightarrow \pi^0 X$ reaction (where X = D or np) at Saskatoon [17]. Most π^0 spectrometers, including the one deployed at Saskatoon, do not have sufficient energy resolution to determine whether this reaction was coherent (X = D) or not (X=np). For the Saskatoon experiment the smaller incoherent cross section was calculated with a model and subtracted from the data to produce a coherent cross section to compare with theory [17].

In general studies of the coherent $\gamma D \rightarrow \pi^0 D$ reaction are best performed with recoil deuteron detection. This is an important opportunity for polarized internal targets which are thin and allow the detection of low energy recoil deuterons. There are also opportunities in the Δ region. There an interesting sensitivity to the quadrupole E2 amplitude has

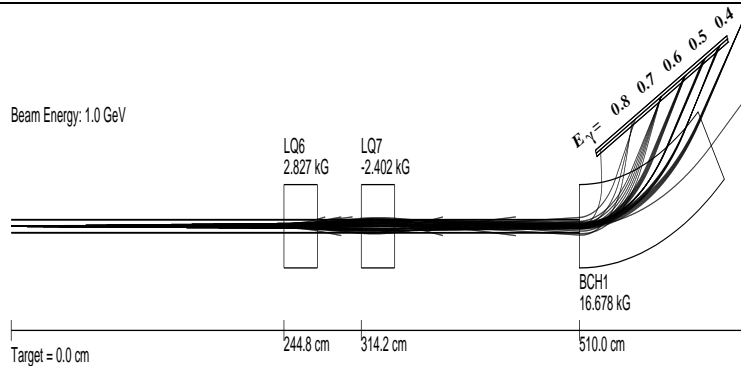
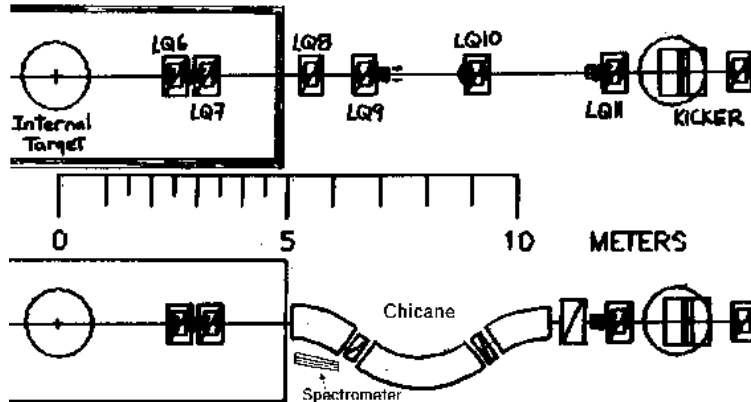


Figure 2: Conceptual layout for a very small angle electron tagging facility at the BLAST target position in the Bates storage ring. The top figure shows where the chicane would fit into the existing ring. The first dipole in the chicane would act as the electron spectrometer. The bottom figure shows sample scattered electron ray bundles (up to $\theta=0.5^\circ$ for $\phi=0,90,180^\circ$). A schematicized wire chamber shows the corresponding almost-real photon energies that would be detected in this zeroth-order design.

been theoretically demonstrated for polarized deuteron targets [18] (see also Fig.10). This sensitivity is for small π^0 CMS angles for which the recoil deuteron energy is small.

Although space does not permit a detailed discussion of Compton scattering, a few remarks about its significance is in order. Previous measurements have aimed to determine the electric and magnetic polarizability of the proton. However, the spin dependent polarizabilities have yet to be measured. These spin dependent polarizabilities are subtle probes of the internal structure of the nucleon. This requires Compton scattering of polarized photons from polarized targets. The use of polarized internal targets is an excellent way to make these measurements, particularly since these targets are thin and one can measure the recoil nuclei as will be discussed in the next section.

2 SMASH: *SM*all Angle Electron Scattering *H*odoscope

In this section we discuss the technique of very small angle electron scattering, or almost–real photon tagging, with a specific conceptual implementation for the Bates Storage Ring, and some ideas for important possible experiments. Much of this material has been presented in an unpublished report from a previous incarnation of this concept proposed at Bates several years ago [19]. This previous project was conceived before BLAST was funded, and therefore was presented as a stand–alone facility with a different proposed position in the Bates Ring. With the advent of BLAST funding, the new idea is to employ the BLAST polarized target, and to make modifications to the ring to accommodate a very small angle electron tagger.

The method of very small angle electron scattering has been known for many years (see e.g. Ref.[20]) and is based on the fact that the virtual photons have very low q^2 , so can be treated as almost–real photons. What is new about the present proposal is the utilization of full polarization observables for both the photon and the target, which is made possible by detecting these very small angle scattered electrons, thereby *tagging* the almost–real exchange photons. The target polarization is made possible by the use of internal targets. For the photon, one obtains circular polarization from longitudinally polarized electrons. The equivalent response function for linear polarized almost–real photons [15] are obtained by measuring the ϕ dependence of the cross section[19]. Therefore, this virtual tagging proposal goes much further in utilizing the polarized, pure, and windowless nature of internal targets, and the very large linear polarization of the almost–real photons.

2.1 Almost-real Photon Tagger

A method to perform very small angle electron scattering/almost–real photon tagging in the Bates Storage Ring is presented in Fig. 2. At this stage the design is conceptual only, but it does exhibit the main features of what a fully designed facility would have. The point here is to introduce the idea and its possibilities to motivate further study.

The design is based on the introduction of a chicane downstream of the internal target position, beginning just outside the BLAST superstructure. A crucial element in the chicane design is that the extra path length introduced must be $n \cdot \lambda = 10.497cm$, where λ is the beam wavelength fixed by the RF. In this conceptual design $n = 5$. Another important element is for the optics from the chicane to the next ring dipole to be identical to the unmodified ring. The chicane shown in Fig.2 does not satisfy this, but preliminary ring optics investigations by T. Zwart of Bates [21] using box (not sector) dipoles without the quadrupoles in between show that in principle this should be possible with relatively minor adjustments of local beam line elements. A full study of this issue could not be completed in time for this article, but nevertheless, one does not expect that the properties of the fully designed chicane/tagger will be significantly different from what is to be described.

Beam electrons which do not interact in the target will be transported around the

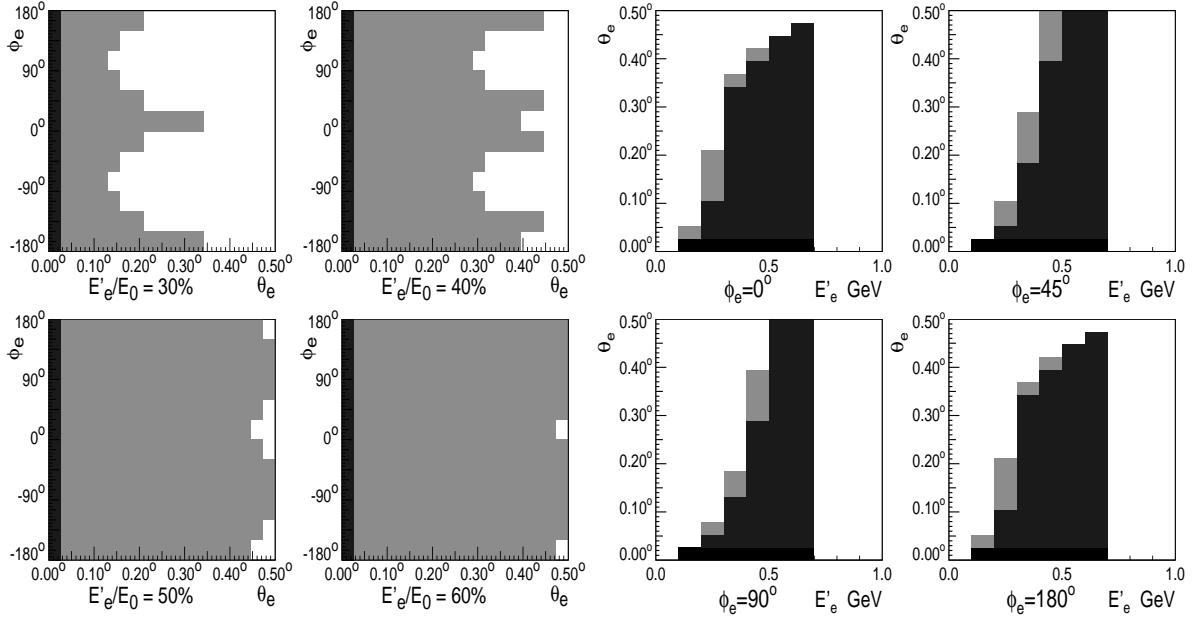


Figure 3: Acceptance of very small angle scattered electrons for the chicane spectrometer design in Fig.2, **Left:** ϕ_e vs θ_e at fixed energy, and **Right:** θ_e vs E' at fixed azimuthal angle. The lightly shaded areas at right indicate partially filled bins.

chicane and then returned to the original ring trajectory. However, the electrons that interact and are scattered into a very small angle ($< 0.5^\circ$ here) will have lost energy, so will be bent away from the beam at the first chicane dipole (see Fig.2). By placing wire chambers to detect these scattered electrons outside this dipole, a QGD spectrometer will be realized. A ray tracing simulation shown in Fig.2 shows that something approximating a focal plane emerges from even this simple design. One is confident then that with a carefully designed first chicane dipole a spectrometer with reasonable optical properties can be achieved.

As a guideline to what can be expected in a full-fledged system, the acceptance of the chicane system (Fig.2) is shown in Fig.3 as a function of the ratio of the outgoing to incident electron energy E'/E , and the outgoing electron angles θ_e, ϕ_e . The acceptance is limited by the apertures of the first two quadrupoles. In this case a rectangular beam box was used, which increases the acceptance at $\phi = 0, 90, 180, 270^\circ$. With the usual cylindrical beam pipe, the acceptance is limited to about 0.33° . Clearly, larger aperture quadrupoles would be preferable, but nonetheless even in this scenario decent momentum coverage is achieved, and as will be shown, a $\simeq 0.5^\circ$ angular acceptance is not unreasonable for almost-real photon tagging.

Here we recall the formulas for the kinematic variables relevant to small angle electron scattering. Note that in the extreme forward direction, the finite mass of the electron cannot be neglected, so the exact expressions must be used. These are [19]:

$$q^2 = -Q^2 = 2m_e^2 - 2EE' + 2pp' \cos\theta_e$$

$$\begin{aligned}
k_\gamma &= \sqrt{p^2 + p'^2 - 2pp' \cos\theta_e} \\
\epsilon &= \left(1 + \frac{Q^2 |k_\gamma|^2}{2p^2 p'^2 \sin^2\theta_e}\right)^{-1} \\
P_\gamma &= h \cdot \sqrt{1 - \epsilon^2} \\
\Gamma &= \frac{\alpha}{2\pi^2} \frac{E'}{E} \frac{k_\gamma}{Q^2} \frac{1}{1 - \epsilon}
\end{aligned}$$

where θ_e is the electron scattering angle, $E(E')$ and $p(p')$ are the beam energy and momentum of the incident (scattered) electrons, h is the longitudinal beam polarization, and q^2 , k_γ , ϵ , P_γ , and Γ are the virtual photon four-momentum, momentum, transverse polarization, circular polarization, and flux, respectively. These formulas still neglect radiative corrections, but these should be relatively small, at the 1% level.

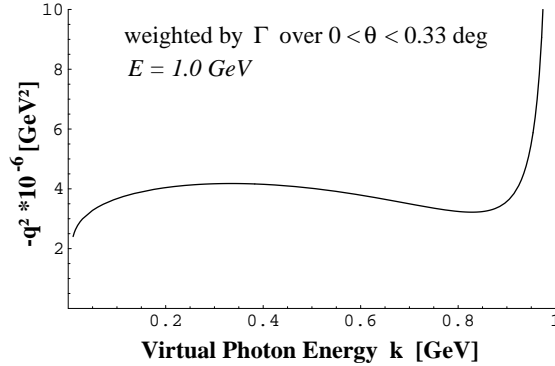


Figure 4: Four-momentum transfer of very small angle scattered 1 GeV electrons versus virtual photon energy, averaged over $\theta < \frac{1}{3}^\circ$ and weighted by the virtual photon flux Γ . Note that these virtual photons are essentially real, except those in the untaggable region very near the endpoint.

Figure 4 shows the four-momentum transfer of the detected scattered electrons, averaged over a $0 < \theta_e < 0.33^\circ$ acceptance and weighted by the virtual photon flux. The very small values indicate that the exchanged virtual photons are essentially real, except very near the endpoint, which nevertheless fall outside the tagging region.

The transverse polarization of almost-real photons are shown in Fig.5 both as a function of scattering angle at fixed photon energy, and also versus energy averaged over angle weighted by the virtual photon flux. Note the very high transverse polarizations over the entire tagging range, averaging about 70%. Note as well that the polarization is constant after about 0.1° . Also shown in Fig.5 is the transferred circular polarization, assuming a 70% longitudinally polarized electron beam. Sizable polarizations which are very flat with angle are seen here as well.

The virtual photon flux is shown in Fig.6, multiplied by the luminosity $7.5 \cdot 10^{31} \text{ cm}^{-2}$, which is what is expected at BLAST for the internal polarized proton target. The left figure

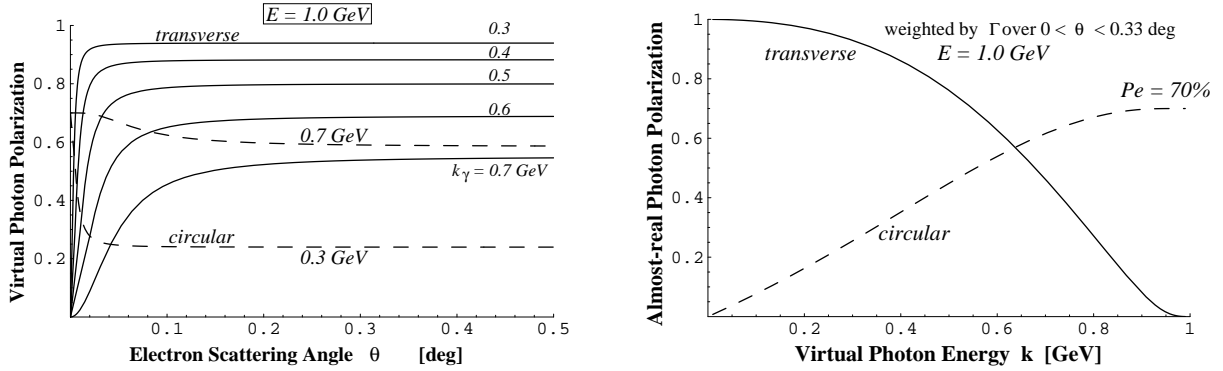


Figure 5: **Left:** Virtual photon polarizations versus electron scattering angle for 1 GeV electrons for various values of photon energy. ; **Right:** Virtual photon polarization versus photon energy, averaged over $\theta < \frac{1}{3}^\circ$ electron scattering angle and weighted by the virtual photon flux Γ . The solid (dashed) line shows the transverse (circular) polarization.

shows the flux versus angle, where it is seen that the flux is strongly forward peaked at most energies, and that there is diminishing strength beyond about 0.5° . Although a larger angular acceptance is clearly preferable, especially for the highest photon energies, this shows that the returns are diminishing beyond this range. The total flux versus photon energy is also shown at right in Fig.6.

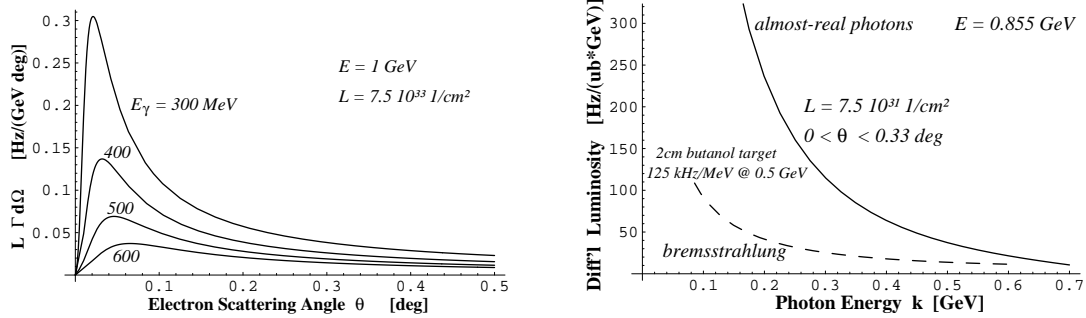


Figure 6: **Left:** Virtual photon rate versus electron scattering angle, for a 1 GeV beam of luminosity $7.5 \cdot 10^{31}$ expected for the BLAST internal polarized proton target. **Right:** Virtual photon flux integrated over $0 < \theta < 0.33^\circ$ solid angle versus virtual photon energy, for the same luminosity at 0.855 GeV. Also shown is the bremsstrahlung rate at that energy expected from the Mainz tagged photon facility, assuming a 2cm polarized butanol target.

The incoherent bremsstrahlung flux assuming a 2cm butanol target from a modern tagged photon facility at Mainz [23] is shown as the dotted line in Fig.6. As well, the energy and linear polarization spectrum of coherent bremsstrahlung beam using a diamond radiator is shown in Fig.7. The former figure demonstrates that even with a thin internal

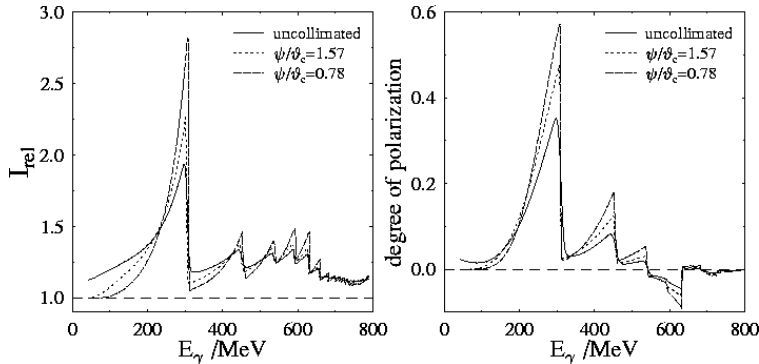


Figure 7: **Left:** Ratio of coherent bremsstrahlung spectrum from a diamond radiator to the incoherent spectrum at $E_0=0.855$ GeV, and **Right:** degree of linear polarization, as a function of photon energy, at the Mainz tagged photon facility (see Ref. [23]). Note that here the linear polarization is sizable in only a narrow energy range, unlike that shown in Fig.5.

target, a sizable rate advantage is seen using tagged almost-real photons, especially for $\frac{E_\gamma}{E_0} < 0.5$. Moreover, low energy recoils are not accessible with usual (thick) frozen targets like butanol, whereas they are with (thin) internal targets. The coherent bremsstrahlung linear polarization spectrum (Fig.7) shows lower polarizations over a much smaller energy range than those in almost-real photon tagging (Fig.5).

The afore described figures demonstrate the salient features of a very small angle electron spectrometer of the kind shown in Fig.2. Namely, it tags virtual photons which are essentially "real" with high transverse and circular polarizations, and a large flux. Coupled with thin highly polarized internal targets, and a versatile detector such as BLAST, supplemented with a hodoscope for low energy recoils (such as a large coverage Si strip counter), it is clear that an almost-real photon tagger opens up many new opportunities. Some examples will be described in the following section.

2.2 Example Experiments

Here a few example experiments will be discussed, focusing on those previously mentioned in conjunction with the chiral dynamics studies outlined in the introduction. Note that the experimental details have not been worked out in time for this contribution, so only a broad outline of what is required will be offered to motivate future study.

Figure 8 shows the recoil proton momentum versus lab scattering angle in the $\gamma p \rightarrow \pi^0 p$ reaction for constant photon energy and constant CMS pion scattering angle. One observes that near threshold the protons recoil at low energy in a forward cone, so that to detect these a forward detector must be constructed. Given the constraints of the BLAST internal target, this detector would probably need to be compact, therefore of high positional reso-

lution, implying a silicon strip-type unit of the kind used in many high energy experiments. Note that thin windowless internal targets have the great advantage here of allowing the low momentum recoils to be detected with minimal interference. One way to identify the scattered π^0 s is to detect the recoil protons with sufficient energy and angular resolution to determine the missing mass. Another is to detect the produced π^0 s, and for this a crystal "ball" or "cylinder" could be constructed to fit around the target. This would greatly reduce backgrounds and add flexibility. It would probably necessitate operating with the BLAST detector "pulled apart", or else BLAST could remain in place and photon detectors installed outside the magnet, but this option increases the size and cost, and reduces the solid angle.

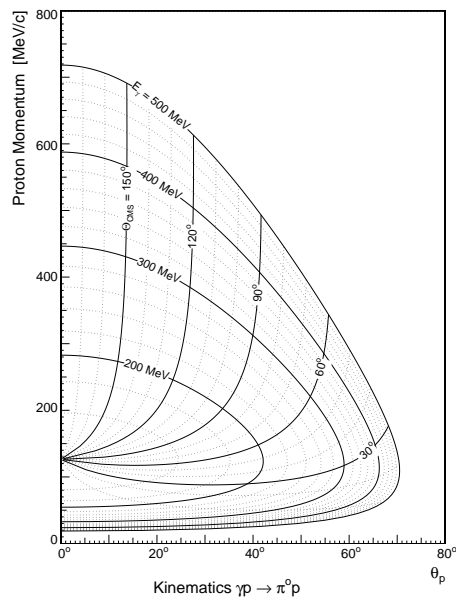


Figure 8: Proton momentum versus scattering angle in neutral pion photoproduction near threshold, with contours of constant photon energy and pion CMS angle. Note that close to threshold the protons recoil forward $< 20^\circ$.

The same Fig.8 can be used to show the kinematics for the $\gamma p \rightarrow \pi^+ n$ reaction, although due to the final state mass differences, the threshold and kinematic contours will be slightly altered. In this case one could use the BLAST detector for π^+ detection with good angular coverage. The planned neutron detector would cover $38 < \theta_n < 70^\circ$, which would cover nicely the Δ resonance region for e.g. $\gamma p \rightarrow \Delta$ studies. However, this precludes the near threshold region, so these detectors would need to be shifted somewhat, or new detectors constructed, to cover the more forward angles.

The proton and photon kinematic relationships for Compton scattering at $E_\gamma = 100 \text{ MeV}$ are shown in Fig.9. This experiment would use the same or very similar setup to that used for the near threshold $\gamma p \rightarrow \pi^0 p$ experiment described above to detect the scattered photon and recoil proton. In addition, near forward photon angles are of interest in double-polarized Compton scattering (see reference [19]). Here, the proton momentum is low and the angle

large, and so can be detected with the proposed BLAST low energy recoil detector [22]. Again, in both cases the thin windowless internal target is seen to be greatly advantageous to facilitate low energy proton detection. Circularly polarized photons are required, and we have seen (Fig.5) that these can be rather sizable.

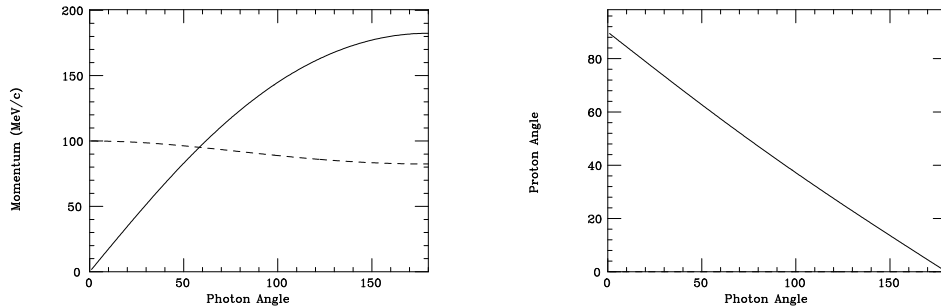


Figure 9: **Left:** Proton and photon momentum versus photon lab angle for Compton scattering at $E_\gamma = 100\text{MeV}$, and **Right:** Angular correlation of the scattered photon and recoil proton.

For a final example, consider the coherent $\gamma D \rightarrow \pi^0 D$ reaction on a vector polarized deuteron target which has been shown (see [19]) to be sensitive to the nucleon quadrupole E2 amplitude. Figure 10 demonstrates the calculated sensitivity, which is greatest at small pion CMS angles where the recoil deuteron energy is low. Again the proposed BLAST low energy recoil detector would be used to detect these deuterons. The neutral pions would be detected with the same setup used for the threshold photoproduction and Compton scattering experiments. Once again the merits of a thin windowless internal target is seen.

3 Conclusion

The experiments presented in the previous section are but a few examples of what can be done to exploit the unique capability of an almost-real photon tagger coupled with the proposed BLAST facility [22]. Including also a new forward hadron detector and a large acceptance photon detector would not only allow three important Chiral Dynamics experiments to be done, but should also open up a whole new arena of unique experiments. The low energy QCD experiments include : threshold photo- π^0 production on polarized protons to measure $Im(E_{0+})$ which is sensitive to the isospin breaking due to the light quark mass differences, fully polarized Compton scattering, which measures the internal quark helicity structure, and the electric quadrupole contribution to the $\gamma N \rightarrow \Delta$ transitions in the proton and the deuteron. Other reactions not touched on here include photo nucleon and photo pion production from polarized few body nuclei. We believe that this opens a new and exciting window of opportunity for polarized, internal, targets at Bates. More detailed design efforts

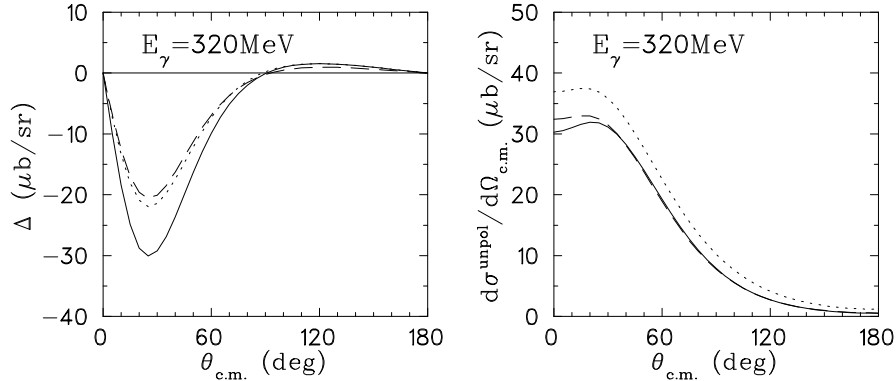


Figure 10: **Left:** Cross section difference ($\sigma \uparrow - \sigma \downarrow$) and **Right:** cross section for coherent π^0 photoproduction on a $\pm 100\%$ vector polarized deuteron target at the Δ energy, from the model described in Ref.[18]. The solid line is the full calculation, whereas the dashed line has the quadrupole E2 amplitude removed. The region of largest sensitivity corresponds to large angle recoil deuterons of a few MeV kinetic energy.

are currently underway, and more input from the collaboration in general would be warmly welcomed.

References

- [1] See e.g. Dynamics of the Standard Model, J. F. Donoghue, E. Golowich, and B. R. Holstein, Cambridge University Press (1992).
- [2] S. Weinberg, Physica A96, 327 (1979). J. Gasser and H. Leutwyler, Ann. Phys. (N.Y.) 158, 142(1984), Nucl. Phys. B250, 465 and 517 (1985). H. Leutwyler, hep-ph/9609465.
- [3] V. Bernard, N. Kaiser, and U.G. Meißner, Int. J. Mod.Phys. E 4, 193 (1995), G.Ecker, Prog. Part. Nucl. Phys. 35, 1 (1995). J.Binnens, G.Ecker, and J.Gasser and other articles in The Second DAPHNE Physics Handbook, L. Maiani, G. Pancheri, and N.Paver, editors (INFN, Frascati (1995))
- [4] Proceedings of the Workshops on Chiral Dynamics: Theory and Experiment, Springer Verlag, July 1998, A.M Bernstein, D. Drechsel, and Th. Walcher, editors, and July 1995, A.M. Bernstein and B. Holstein editors.
- [5] J. Goldstone, Nuovo Cimento **19** (1961) 154.
- [6] H. Leutwyler hep-ph/9409422 and hep/ph/9609466.
- [7] S. Weinberg, Transactions of the N.Y. Academy of Science Series II 38 (I.I. Rabi Festschrift),185 (1977),and contribution to[4].

- [8] J. Gasser and H. Leutwyler, Phys. Rep. **87** (1982) 77 ; H. Leutwyler, hep-ph/9602255, and Phys. Lett. **B378** (1996) p313.
- [9] S. Weinberg, Phys. Rev. Lett. **17** (1966) 168.
- [10] A. M. Bernstein et al., Phys. Rev. **C55** (1997) 1509 ; M. Fuchs. et al., Phys. Lett., **B368** (1996) 20.
- [11] J.C. Bergstrom, et al., Phys. Rev. **C53** (1996) R105 ; Phys. Rev. **C55** (1997) 2016.
- [12] V. Bernard, N. Kaiser, and U.G. Meißner, Int. J. Mod. Phys. E4, 193 (1995), Nucl. Phys. **B383** (1992) 442 ; Phys. Rev. Lett. **74** (1995) 3752 ; Z. für Physik **C70** (1996) 483 ; Phys. Lett. **B378** (1996) 337.
- [13] A.M. Bernstein, πN Newsletter No. 11, Dec. 1995 ; Proceedings of the PANIC Conference, C.E. Carlson and J.J. Domingo editors, World Scientific, Singapore, 1996 ; and to be published.
- [14] D. Sigg et. al., Phys. Rev. Lett. **75** (1995) 3245 ; Nucl. Phys. **A609** (1996) 269 ; **A617** (1997) 526 ; A. Badertscher, in proceedings of the Workshop on Chiral Dynamics, Mainz. Sept 1-5, 1997, A.M. Bernstein, D. Drechsel, and Th. Walcher, editors, Springer-Verlag, in press ; and private communication.
- [15] D. Drechsel and L. Tiator, J. Phys. G: Nucl. Part. Phys. **18** (1992) 449 ; A.S. Raskin and T.W. Donnelly, Annals of Phys. **191** (1989) 78.
- [16] S. Beane, V. Bernard, T.S.H. Lee, U.G. Meißner, U. van Kolck, Nucl. Phys. **A618** (1997) 381.
- [17] J.Bergstrom, et al., Phys. Rev. **C57** (1998) 3203.
- [18] P. Wilhelm and H. Arenhovel, Nucl.Phys. **A609** (1996) 469.
- [19] Polarized Internal Target Experiment, Preliminary Design Report, A.M Bernstein et al., March 1996, unpublished. A Postscript version can be found at the WWW page: <http://pierre.mit.edu/~mpavan/> .
- [20] C.E. Hyde-Wright, W. Bertozzi, J.M. Finn, MIT/LNS internal report DOE/ER 03065-3571, *circa* 1982.
- [21] Townsend Zwart, private communication, June 1998.
- [22] BATES BLAST Technical Design Report, Aug.8, 1997, unpublished.
- [23] see MAMI A2 Collaboration Annual Report 1996, available at WWW page <http://www.kph.uni-mainz.de/A2/a2jabe96e/a2jabe96e.html> .